Structure and Properties of $Ba_6Ni_{25}S_{27}$

M. C. Gelabert, M. H. Ho, A.-S. Malik, F. J. DiSalvo,* P. Deniard, and R. Brec

Abstract: $Ba_6Ni_{25}S_{27}$, synthesized by solid-state reaction of BaS, NiS, and Ni at 675 °C, is cubic ($Pm\bar{3}m$, $a = 10.057(1)$ Å). The structure was refined by using powder X-ray diffraction and Rietveld methods with $R_p = 6.28\%$, $R_{wp} = 8.13\%$, $\chi^2 = 3.120$. The structure, isotypic with $Ba_6Co_{25}S_{27}$, consists of an extended network of Ni_8S_{14} pseudo-cube clusters, NiS_6 octahedra, and Ba_6S octahedra. Extended Hückel calculations of this compound indicate the band structure near the Fermi level to be composed mostly of d-character orbitals of tetrahedral Ni, and reveal a peak in the density of states slightly below the Fermi level. The temperature dependence of the electrical resistivity exhibits a local maximum with thermal hysteresis at around 230 K. Above and below this transition, the slope of the resistivity is positive, with a room-temperature resistivity ($\rho = 0.23$ mΩcm) in the range for that of a poor metal conductor. Magnetic susceptibility measurements from 4 to 900 K indicate a sharp change in slope at around 225 K, with a steadily increasing susceptibility up to 900 K. The susceptibility below 225 K suggests Pauli paramagnetic behavior. Low-temperature powder X-ray diffraction and subsequent structure refinement shows that the lattice parameter, a, undergoes a slight change in slope at temperatures of around 235 K.

Keywords
conducting materials · electronic structure · magnetic properties · phase transitions · sulfur

Introduction

Many of the ternary phase diagrams between alkaline earth metals, late transition metals (Fe, Co, Ni, Cu, Zn), and chalcogens comprise a small number of phases, and all contain only a few ternary compounds, except for Ba–Fe–S, whose phases number about 20.[1–5] Virtually all of the compounds in this system contain FeS_4 tetrahedra as the primary units, either isolated or connected by the corners or edges. The structures of these phases range from infinite chains of edge-sharing tetrahedra to isolated single tetrahedra; many motifs exist that are between these two extremes. Most of these compounds are insulating and antiferromagnetic. Only three barium cobalt sulfides have been reported: 1) metallic $Ba_6Co_{25}S_{27}$;[6] 2) $BaCoS_2$,[7–9] a Mott–Hubbard insulator with distorted square-pyramidal Co coordination; and 3) Ba_2CoS_3,[10] an antiferromagnetic insulator that contains only tetrahedrally coordinated Co. In the Ba–Cu–S system there are two diamagnetic phases, of which one, $BaCu_2S_2$,[11–13] contains Cu in tetrahedral coordination and the other, $BaCu_4S_3$,[11,14] has two polymorphs and contains tetrahedrally and trigonally coordinated Cu. In the barium zinc sulfides there is only one phase, Ba_2ZnS_3, which contains tetrahedrally coordinated Zn.[15]

The Ba–Ni–S phase diagram contains just two ternary compounds: metallic $BaNiS_2$, first reported as a new structure type in 1970,[16] and $Ba_6Ni_{25}S_{27}$. In $BaNiS_2$, Ni is in a square-pyramidal environment of sulfur; these pyramids are edge-sharing in an *anti* configuration to form square $[NiS_{4/4}S]^{2-}$ sheets, with Ba^{2+} above and below each pyramid. $Ba_6Ni_{25}S_{27}$ was first mentioned in an article about $Ba_6Co_{25}S_{27}$; attempts to synthesize $Ba_6Ni_{25}S_{27}$ resulted in multiphase products.[6] Here, the synthesis conditions necessary to produce single-phase material are described, as well as electrical resistivity and magnetic susceptibility measurements. Powder X-ray diffraction data were used in the structure refinement. A phase transition, observed in the resistivity and susceptibility measurements, prompted some variable-temperature X-ray powder diffraction work in order to determine whether this phenomenon is structural in origin. Extended Hückel calculations on the refined structure were performed.

Experimental Procedure

Commercial BaS (Cerac 99.8% metals basis) was used in several reactions first. For the final few syntheses, BaS was synthesized from the elements in dry liquid ammonia by a similar procedure to that used for K_2S.[17] NiS was synthesized from the elements (Ni, Alfa–Aesar 4N6; S, Metalspecialties 5N5). Before this synthesis, the Ni was reduced under a hydrogen stream at 600 °C; this treatment resulted in a negligible mass loss, demonstrating that the Ni did not contain much NiO or $Ni(OH)_2$ contamination.

Stoichiometric quantities (BaS/NiS/Ni = 6:21:4) of the sulfides (total mass 0.4 g) and Ni were ground into a fine powder, pelletized, and placed in a

[*] F. J. DiSalvo, M. C. Gelabert,[+] M. H. Ho, A.-S. Malik
Department of Chemistry, Cornell University
Ithaca, NY 14853-1301 (USA)
Fax: Int. code +(607)255-4137
e-mail: fjd3@cornell.edu
P. Deniard, R. Brec
Laboratoire de Chimie des Solides, I. M. N.
2 rue de la Houssinière, 44072 Nantes, Cedex 03 (France)
[+] Current address: Department of Ceramic Engineering
Rutgers State University of New Jersey, Piscataway, NJ 08855 (USA)

0947-6539/97/0311-1884 $ 17.50+.50/0

graphite crucible, which was then sealed in an evacuated quartz tube (< 5 mtorr). The tubes were taken to 675 °C over 8 h, held at that temperature for three days, and allowed to cool slowly with the furnace. The initial products were ground, pelletized, and reheated at least once to ensure sample homogeneity. The single-phase product had a reddish-purple color.

Attempts to synthesize this material at a temperature greater than 675 °C resulted in a mixture of $Ba_6Ni_{25}S_{27}$, $BaNiS_2$, and NiS, observed by powder X-ray diffraction. Thermodynamically, this phase has an upper limit of stability around this temperature; by 700 °C, significant melting occurs and reflections from $BaNiS_2$ and NiS begin to appear in the X-ray diffraction patterns.

Room-temperature powder X-ray diffraction data were collected on a Scintag 2000 diffractometer with $Cu_{K\alpha}$ radiation in a $\theta-\theta$ geometry. Sintered powder was passed through several meshes, to give a final particle size of 37 μm. A data set was collected over the range $5 \leq 2\theta \leq 100°$ for Rietveld analysis, using a step size of 0.03° and a time per step of 20 s.

Low-temperature powder X-ray diffraction was performed on a Siemens 5000 diffractometer with $Cu_{K\alpha}$ radiation in a $\theta-\theta$ geometry. Sintered powder was passed through several meshes, to give a final particle size of 40 μm. Data sets were then collected over the range $133 < T < 293$ K in 20 K increments; powder histograms were collected over $10 \leq 2\theta \leq 100°$ for Rietveld analysis, using a step size of 0.03° and a time per step of 50 s.

For the room-temperature data, lattice parameters were first determined with the Scintag peakfinder and $K_{\alpha 2}$ stripping routines found in the VMS software.[18] A least-squares fit to the lattice parameter was subsequently found by means of a refinement code written in our laboratories. This lattice parameter was also used for the low-temperature structure refinements. Since the reflections in the powder pattern could be indexed exactly to that of $Ba_6Co_{25}S_{27}$, the same space group ($Pm\bar{3}m$) and atomic positions were used for the structural model. Out of all the cubic space groups, there is only one other, $Pm\bar{3}$, that is primitive and retains a center of symmetry. Refinement in this latter space group proved to be significantly less stable at high and low temperatures.

GSAS software was used to refine the structure[19] for all temperatures. For the low-temperature data, the shifted Chebyshev polynomial function was used for the background. The powder used for the low-temperature data collection had a small (2–3%) NiS impurity, which was refined together with $Ba_6Ni_{25}S_{27}$. The refined structures from pure and impure powder were identical within conservative standard deviations. The pseudovoigt peak function was refined along with lattice parameters, z and polarization corrections, atomic coordinates, and isotropic thermal parameters.

The 8 mm diameter pellet for electrical resistivity measurements was sintered from single-phase powder at 675 °C for one day and cooled slowly. The product had a smooth surface and homogeneous color. Resistance was measured at 18.0 Hz by means of a four-probe AC apparatus with lock-in detection. Spring-loaded gold pins were used to make electrical contact to the pellet, and a machined molybdenum standard of the same diameter and similar thickness was measured to determine the geometrical conversion factor to resistivity. It was found that the $I-V$ characteristic was linear over a current range of 80–400 mA, and that the contact resistances were less than 1 Ω.

Magnetic susceptibility from 4 to 900 K was measured on an 85.3 mg sample of polycrystalline powder with a Faraday microbalance, in a previously calibrated system.[20] The field dependence of the susceptibility was measured from 0.2 to 1.2 T at room temperature and at 4 K. A plot of the gram susceptibility versus $1/H$ showed a decrease of about 6% over the measured field range, indicating a very small contribution from ferromagnetic impurities. At 4.2 K, the susceptibility differed by about 18% over the field range. The room-temperature value of the magnetic susceptibility extrapolated to infinite field is 1.80×10^{-6} emu g^{-1}. This extrapolation eliminates the contribution to the susceptibility from ferromagnetic contamination, and this correction was applied to all data.

Results

Details of the data collection and Rietveld refinement at room temperature are summarized in Table 1 and Figure 1. A pseudovoigt function was used to fit the peak profiles. The atomic parameters and isotropic thermal parameters (Table 2) behaved reasonably well; in the last stages of the refinement, both were varied simultaneously without producing a noticeable change in either parameter. The atomic positions did not deviate significantly from those of $Ba_6Co_{25}S_{27}$, whose structure was determined by single crystal X-ray diffraction.[6]

The structure of $Ba_6Ni_{25}S_{27}$ can most easily be envisaged as the coordination of the two crystallographically distinct Ni atoms in the structure (Figure 2). Ni1 is octahedrally coordinated by S2; these NiS_6 octahedra are at the corners of the cell. The Ni2 atoms form tetragonally distorted cubes that are face-

Table 1. Collection and refinement parameters for X-ray powder diffraction data recorded at room temperature.

empirical formula	$Ba_6Ni_{25}S_{27}$
formula weight	3157.52 g mol^{-1}
crystal system	cubic
space group	$Pm\bar{3}m$
a	10.0565(2) Å
V	1017.03(7) Å^3
Z	1
ρ (calculated)	5.155 g cm^{-3}
radiation	$Cu_{K\alpha}$
λ_1, λ_2	1.5405, 1.5443 Å
T	293(2) K
2θ	5–100°
step size, time/step	0.03°, 20 s
no. of data points	3167
no. of reflections	84
parameters	49
background function	cosine fourier series
profile function	pseudovoigt
Gaussian and Lorentzian fractions	GW = 1.049, LX = 6.138
transparency coefficient	0.6989
asymmetry term	0.9298
R_p	0.0628
R_{wp}	0.0813
χ^2	3.120

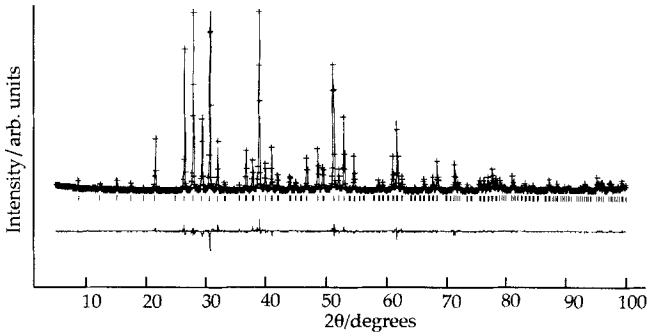

Figure 1. Calculated (solid line), observed (+) and difference plots for powder structure refinement from powder X-ray diffraction data.

Table 2. Atomic coordinates and isotropic thermal parameters for X-ray powder refinement in space group $Pm\bar{3}m$.

Atom	Wyckoff symbol	x	y	z	U_{iso} (Å^2)
Ba	*6f*	1/2	1/2	0.1945(2)	0.019(2)
Ni1	*1a*	0	0	0	0.035(4)
Ni2	*24m*	0.1360(2)	0.3562(2)	0.1360(2)	0.033(3)
S1	*1b*	1/2	1/2	1/2	0.026(6)
S2	*6e*	0	0.2377(5)	0	0.019(3)
S3	*8g*	0.2822(3)	0.2822(3)	0.2822(3)	0.028(3)
S4	*12h*	0	1/2	0.2416(4)	0.020(2)

  0947-6539/97/0311-1885 $ 17.50+.50/0

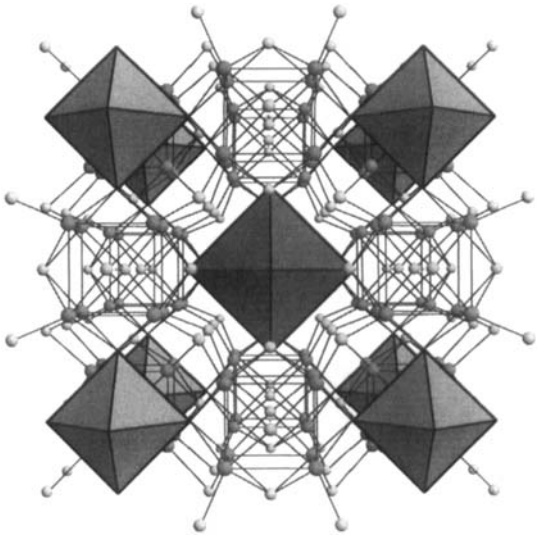

Figure 2. Structure of $Ba_6Ni_{25}S_{27}$, with the dark Ba_6S octahedron in the middle and the light NiS_6 octahedra at the corners of the unit cell. The large spheres are Ni atoms, which form Ni_8 pseudo-cubes that are face- and corner-capped by sulfur atoms (*small spheres*).

capped by S2 and S4, and corner-capped by S3, making Ni_8S_{14} clusters (Figure 3); the coordination of Ni2 by sulfur is approximately tetrahedral. These Ni_8S_{14} clusters sit at the middle of the edges of the unit cell, and share S2 with the Ni1 octahedra. Finally, in the middle of the unit cell is S1 surrounded by six Ba atoms in an octahedral environment. This structure can be related to that of perovskite[6] by considering the placement of the pseudocubes and octahedra in the cubic unit cell. Along all three [100] directions of this structure, NiS_6 octahedra alternate with Ni_8S_{14} cubes to form chains, and Ba_6S fills the dodecahedral holes in the cluster framework.

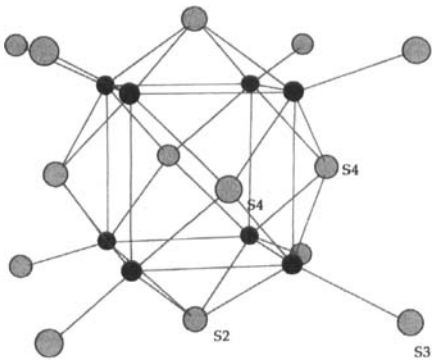

Figure 3. Ni_8S_{14} cube cluster arrangement in $Ba_6Ni_{25}S_{27}$. The dark spheres represent Ni2, and the light spheres S. Crystallographically distinct sulfur atoms are labeled.

Important bond lengths and angles for the room-temperature structure are listed in Table 3. Ni–S bond lengths in other compounds vary significantly with Ni coordination and defect density. For tetrahedral Ni, as found in Ni_3S_2 (albeit significantly distorted), values range from 2.25 to 2.29 Å.[21] Square-pyramidal coordination, found in $BaNiS_2$, yields bond lengths of 2.32 to 2.35 Å.[16] In octahedral coordination, as found in NiS_2 and hexagonal NiS,[22] the distances range from 2.39 to 2.40 Å. The Ni–S distances in rhombohedral millerite (NiS) are 2.30 Å.[23] In the binary nickel sulfides, there exist many other phases, such as Ni_7S_6,[24] $Ni_{17}S_{18}$,[25] and Ni_3S_2,[21] which contain unusual or severely distorted Ni coordination, ordered defects, or metal–metal bonding; these in turn produce a large overall range of Ni–S distances (2.15–2.56 Å). The Ni–S tetrahedral (2.21–2.27 Å) and octahedral (2.39 Å) bond lengths in $Ba_6Ni_{25}S_{27}$ compare well with those of the above-mentioned binary and ternary phases. In $Ba_6Co_{25}S_{27}$, the octahedral and tetrahedral Co–S bond lengths also vary in a similar way. The Ba–S distances (3.07–3.25 Å) in $Ba_6Ni_{25}S_{27}$ are comparable with those in Ba–S phases (3.11–3.54 Å), $BaNiS_2$ (3.10–3.50 Å), and $Ba_6Co_{25}S_{27}$ (3.05–3.27 Å).

Table 3. Selected bond lengths (Å) and angles (°) for $Ba_6Ni_{25}S_{27}$.

Ba-S1	3.072	S2-Ni2-S3	128.7
Ba1-S3 ×4	3.221	S2-Ni2-S4	104.7
Ba1-S4 ×4	3.253	S3-Ni2-S4	107.8
Ni1-S2 ×6	2.390	S4-Ni2-S4	99.21
Ni2-S2	2.272	Ni1-S2-Ni2	121.6
Ni2-S3	2.208	Ni2-S3-Ni2	90.34
Ni2-S4 ×2	2.256		
Ni2-Ni2 ×2	2.736		
Ni2-Ni2	2.892		
Ni2-Ni2	3.132		

The room-temperature resistivity of this material was determined to be 0.232(7) mΩcm, about two orders of magnitude higher than that of pure copper metal; this value is in the range expected for a poor metal conductor. The temperature dependence from 4 to 350 K (Figure 4) displays metal-like behavior

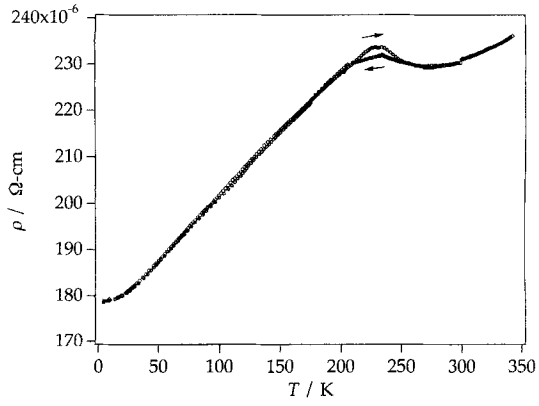

Figure 4. Electrical resistivity versus temperature for a sintered, polycrystalline pellet.

(positive slope) throughout most of the temperature range (4–230 K). Around 230 K there is a broad anomaly in the resistivity, which exhibits thermal hysteresis.

Magnetic susceptibility data as a function of temperature (Figure 5) display a Curie tail at low temperatures. At 225 K there is a break in slope, which correlates very well with the first-order phase transition seen in the resistivity data.

Fitting the low-temperature susceptibility data to the Curie–Weiss law [Eq. (1)] over the range $40 < T < 230$ K yields

$$\chi = \chi_0 + \frac{C}{(T+\theta)} \quad (1)$$

0947-6539/97/0311-1886 $ 17.50+.50/0 *Chem. Eur. J.* **1997**, *3*, No. 11

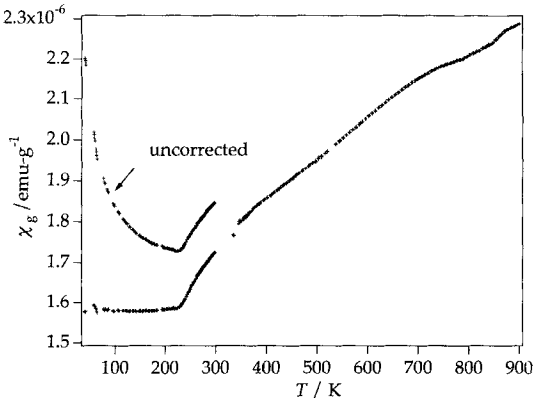

Figure 5. Magnetic susceptibility vs. temperature. The uncorrected low-temperature data are shown, as well as values obtained by subtracting small ferromagnetic and Curie contributions determined from those data.

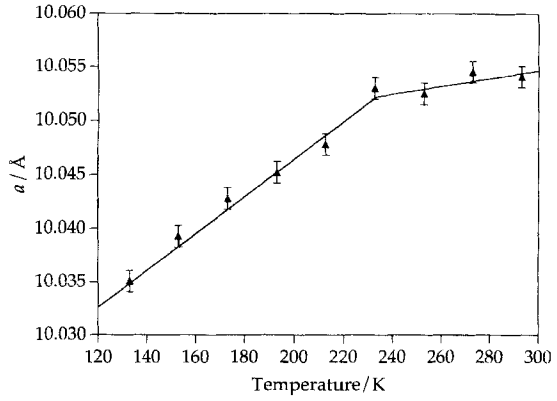

Figure 7. Lattice parameter a as a function of temperature, determined from Rietveld refinements on temperature-dependent powder X-ray diffraction data.

$C = 1.78(6) \times 10^{-5}$ emu K g^{-1}, $\chi_0 = 1.641(3) \times 10^{-6}$ emu g^{-1}, $\theta = -9(1)$ K, and $\mu_{eff}/Ni = 0.134\ \mu_B$. From this Curie constant, the estimated fraction of localized spin ½ moments ($g = 2$) is 0.6%. The calculated fraction is 0.07% for spin 2 and $g = 2$ (assuming paramagnetic Fe impurities); this fraction is somewhat higher than the stated Ni purity of 99.996%. Nevertheless, the fraction of localized moments is small, indicating that the intrinsic susceptibility at low temperatures is temperature-independent, because of the expected Pauli and Van Vleck paramagnetism.

Above 225 K the susceptibility increases steadily from 1.75×10^{-6} to 2.35×10 emu g^{-1} at 890 K. The effective moment per formula weight can be calculated from the formula $\mu_{eff} = (8\chi_M T)^{1/2}$, where χ_M is the molar susceptibility. A graph of this calculated value versus temperature (Figure 6) shows

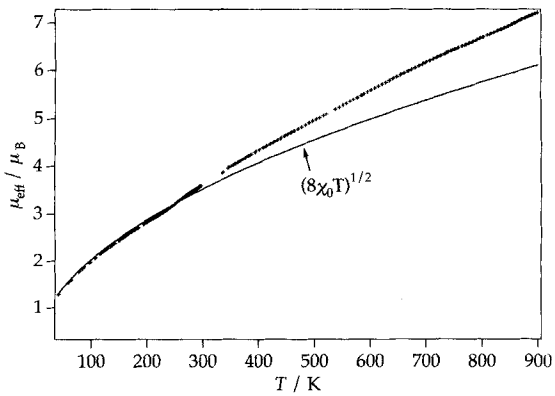

Figure 6. Effective magnetic moment as a function of temperature is estimated from the formula $\mu_{eff} = (8\chi_M T)^{1/2}$, where χ_M is the corrected molar susceptibility. The lower curve was obtained by determining χ_M from χ_0, the temperature-independent susceptibility term from the Curie–Weiss fit to the low-temperature data.

that it increases continuously from 3.0 μ_B at 225 K to 7.2 μ_B at 900 K. If it is assumed that $g = 2$, these values correspond to 12.0 and 69.1% of the Ni, respectively, possessing a localized, spin $^1/_2$ moment.

Lattice parameters and bond lengths were examined carefully as a function of temperature in the region of the anomalies in the resistivity and susceptibility measurements. The lattice parameter a as a function of temperature (Figure 7) shows the usual contraction upon cooling, with a broad rollover at around 237 K. Similar plots of bond lengths indicate that those of Ba–S, Ni–Ni, and Ni–S are only weakly temperature-dependent, as expected for thermal contraction.

Extended Hückel calculations of $Ba_6Ni_{25}S_{27}$ were performed.[26, 27] The total density of states (DOS), along with specific contributions to the DOS, are shown in Figure 8 for the

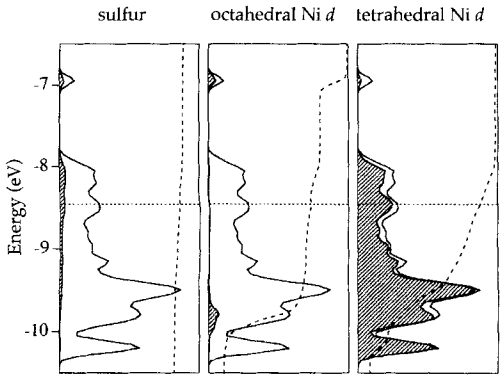

Figure 8. Results of extended Hückel calculations. The total density of states (DOS) is indicated by the solid line; the shaded region is the contribution to the total DOS; the dotted curve is the integration of the specified DOS contribution: the horizontal dotted line is the Fermi level.

energy window from −10.5 to −6.5 eV. The calculations show that most of the contribution to the DOS in the region of the Fermi level is due to the d orbitals of the tetrahedrally coordinated Ni, with very little contribution from S. The d orbitals of the octahedrally coordinated Ni are concentrated above and below the Fermi level, with negligible contribution at the Fermi level. This leads to a calculated oxidation state of +1.8 for the octahedrally coordinated Ni. There is a broad local maximum in the DOS slightly below the Fermi level.

Discussion

The structure of $Ba_6Ni_{25}S_{27}$ is that of djerfisherite.[28–30] Originally found in meteorite deposits, the minerals in this group have been allocated many molecular formulas, including

  0947-6539/97/0311-1887 $ 17.50+.50/0

$K_6(Cu,Fe)_{25}S_{26}Cl$ and $K_6Na(Fe,Cu,Ni)_{24\pm x}S_{26}Cl$.[28] They often contain a different metal for the octahedrally coordinated Ni1, and a Cl atom in place of S1 in the middle of the unit cell. There are many compositional variations that retain this structure type, and most of them occur naturally. This structure is also reminiscent of pentlandite, M_9S_8, which, in nature, is found with mixtures of mostly Fe, Co, and Ni in the M site.[31] Like $Ba_6Ni_{25}S_{27}$, pentlandite also contains transition metal cube clusters and octahedra.

There are two models that may explain the high-temperature susceptibility behavior of $Ba_6Ni_{25}S_{27}$. Despite the observed metallic behavior, a fraction of the available electrons could be localized on the Ni atoms, introducing the possibility of magnetic exchange interactions. The other possibility concerns the presence of a peak in the density of states near the Fermi level, ε_F. The Pauli paramagnetic contribution to the susceptibility is proportional to the DOS, within a few k_BT of ε_F. Thus, the modest peak found in the DOS just below ε_F should increase the Pauli paramagnetic contribution to the susceptibility with increasing temperature.

In order to investigate further the first model, an analysis of the individual exchange pathways within the structure provides some insight into the potential magnetic interactions within this structure. The Ni–Ni distance between tetrahedra and octahedra is 4.071 Å, so the octahedrally coordinated Ni1 is quite isolated compared with the tetrahedral Ni2, and may possess a magnetic moment. However, the effective moment exhibited by this material is too high to be accounted for by this single Ni1 atom. In NiS and NiS_2, octahedrally coordinated Ni is divalent; furthermore, band calculations estimate the octahedral Ni oxidation state to be approximately +II. Therefore, it is reasonable to assert that octahedral Ni in $Ba_6Ni_{25}S_{27}$ is divalent (d^8, spin 1). With a Landé g factor of 2, the effective magnetic moment calculated from such a state is 2.83 μ_B. Although this calculated value is close to the room-temperature measured moment, at high temperatures it is much lower than the average measured magnetic moment per formula unit.

The Ni_8S_{14} pseudo-cube clusters form the same lattice as the anions in the perovskite structure, that of AB-stacked kagomé nets (Figure 9). The magnetic frustration exhibited by this arrangement of sites is well documented. Examples include the oxide pyrochlores,[32] magnetoplumbites,[33] hexagonal ferrites,[34] and cubic Laves phases.[35] Every site shown in Figure 9 is occupied by the cube cluster. The intracluster (edge-sharing) Ni2–Ni2 bond lengths are 2.736 and 2.892 Å (for comparison, the elemental Ni–Ni bond length is 2.49 Å). These values are close enough for significant direct orbital overlap for magnetic exchange within each cluster. This direct interaction may compete with the ever-present superexchange through the sulfur anions. The short intercluster (corner-sharing) Ni2–Ni2 distance of 3.132 Å is also close enough to have some electronic and magnetic interaction through superexchange pathways.

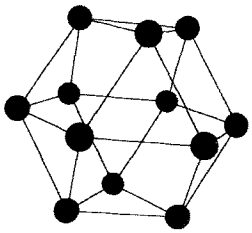

Figure 9. Arrangement of cube clusters in $Ba_6Ni_{25}S_{27}$ ([111] direction perpendicular to the page).

The short Ni–Ni distances within and between these clusters are unquestionably a major contributor to the high conductivity and metallic behavior of $Ba_6Ni_{25}S_{27}$. The domination of these bands at ε_F further supports this conjecture. Potential frustration can easily be observed magnetically within a single (111) layer, by attempting to assign antiferromagnetic spins to adjacent tetrahedra and carrying this over to the next cluster. However, the relationship, if any, between this magnetic structure and the high-temperature susceptibility data is not yet understood. Magnetically frustrated compounds usually exhibit a spin–glass transition at low temperatures, with behavior below this transition depending on the magnetic history of the sample upon cooling. $Ba_6Ni_{25}S_{27}$ shows no such behavior in the magnetic susceptibility data.

If there were Ni moments, the measured susceptibility would be consistent with a large exchange constant between Ni atoms, so that the susceptibility would show a maximum at high temperature due to short- or long-range magnetic order. This was never observed at any temperature up to 890 K, which is just 60 K below the incongruent melting point. The fact that the susceptibility and the effective magnetic moment increase steadily to such a high temperature suggests that the exchange energies would have to be greater than approximately 900 K, or about 0.1 eV.

Given the metallic behavior of this phase, the second model is also possible, namely, that the increase in susceptibility is attributable to structure in the DOS near ε_F. In transition metal compounds, the Pauli susceptibility is often temperature-dependent. $BaNiS_2$, also a poor metallic conductor, exhibits similar susceptibility behavior up to 1000 K.[36] The Ni–Ni bond length of 3.49 Å in $BaNiS_2$ is much longer than that in $Ba_6Ni_{25}S_{27}$. It is interesting to note that if the susceptibility of a metallic system were interpreted as arising from localized moments, the magnitude of such moments ($\mu_{eff} = (8\chi_M T)^{1/2}$) would increase with temperature. However, if χ_M is taken from χ_0, the Pauli term, the curve shown in Figure 6 is obtained. Although similarities between the observed and calculated effective moments exist at low temperature, a significant deviation from the experimental data occurs at high temperatures. The assumption that the magnetic data arise from localized moments may be misleading. Taking this into account, we favor the band model to describe this compound.

The structure change seems quite subtle compared with the transitions observed in resistivity and susceptibility data. The deviation in the lattice parameters as a function of temperature occurs around 237 K, at the intersection of straight-line estimates below and above the transition, with a slope increase below 237 K. The observed lattice-constant change and phase transition upon cooling are within 10 K of each other, and well within the observed range of temperature for the structural change. The slope change at 237 K certainly indicates differences in local bonding interactions, which may produce the significant effects in magnetic and electrical behavior. However, the hysteresis observed in the resistivity data implies the existence of domains which are likely to be structurally different. The changes associated with shifting of these domains may have magnetic consequences independent of any local electronic effects.

0947-6539/97/0311-1888 $ 17.50+.50/0 Chem. Eur. J. 1997, 3, No. 11

The observations seen in this study—the change in temperature dependence of the lattice parameter, the broad resistivity transition, and the sharp change in susceptibility behavior—appear to be highly correlated. The changes in the physical properties of $Ba_6Ni_{25}S_{27}$ at around 230 K are reflected in a change in slope of the plot of lattice parameter versus temperature. At temperatures below 230 K, $Ba_6Ni_{25}S_{27}$ is metallic and shows a temperature-independent susceptibility (Pauli paramagnetism), plus a small Curie "tail" due to localized paramagnetic impurities. The high-temperature behavior of the susceptibility is not completely understood. $Ba_6Ni_{25}S_{27}$ is still metallic even at 350 K; this suggests that the susceptibility behavior at high temperatures is due to an increase in DOS at the Fermi level. Extended Hückel calculations indicate some structure of the DOS near the Fermi level, which supports this explanation for the high-temperature magnetic data. Alternatively, the electrons may become more correlated above 230 K, producing some short-range magnetic order without a magnetic transition. At this point, it is not clear what interactions drive the phase transition observed near 230 K.

The extended clusters found in $Ba_6Ni_{25}S_{27}$ and $Ba_6Co_{25}S_{27}$ are chemically intriguing, because of the different coordinations of the transition metal within one structure and the similarity to related molecular clusters. $Ba_6Co_{25}S_{27}$ is a paramagnetic metallic compound, which has been suggested to have significant electron–electron correlations.[6] Given their unusual structure and properties, these cluster phases are worthy of further study, including more detailed band calculations, ESR, NMR, and neutron diffraction experiments on the parent phases, and chemical substitution investigations.

Acknowledgments: We acknowledge the support of the US Department of Energy (Grant number DE-FG02-87ER45298). MCG is grateful to Simon Clarke for discussions on magnetism.

Received: February 24, 1997 [F621]

[1] S. Cohen, N. Kimizuka, H. Steinfink, *J. Solid State Chem.* **1980**, *35*, 181–186.
[2] S. Cohen, L. E. Rendon-Diazmiron, H. Steinfink, *J. Solid State Chem.* **1978**, *25*, 179–187.
[3] J. T. Hoggins, H. Steinfink, *Acta. Crystallogr. Sect. B* **1977**, *33*, 673–678.
[4] J. T. Lemley, J. M. Jenks, J. T. Hoggins, Z. Eliezer, H. Steinfink, *J. Solid State Chem.* **1976**, *16*, 117–128.
[5] I. E. Grey, *J. Solid State Chem.* **1974**, *11*, 128–134.
[6] G. J. Snyder, M. E. Badding, F. J. DiSalvo, *Inorg. Chem.* **1992**, *31*, 2107–2110.
[7] G. J. Snyder, M. C. Gelabert, F. J. DiSalvo, *J. Solid State Chem.* **1994**, *113*, 355–361.
[8] N. C. Baenziger, L. Grout, L. S. Martinson, J. W. Schweitzer, *Acta Crystallogr. Sect. C* **1994**, *50*, 1375–1377.
[9] M. C. Gelabert, N. E. Brese, F. J. DiSalvo, S. Jobic, P. Deniard, R. Brec, *J. Solid State Chem.* **1996**, *127*, 211–218.
[10] H. Y. Hong, H. Steinfink, *J. Solid State Chem.* **1972**, *5*, 93–104.
[11] A. Ouammou, M. Mouallenn-Bahout, O. Peña, J. Halet, J. Saillard, C. Carel, *J. Solid State Chem.* **1995**, *117*, 73–79.
[12] M. Saeki, M. Onoda, H. Nozaki, *Mater. Res. Bull.* **1988**, *23*, 603–608.
[13] J. Iglesias, K. Pachali, H. Steinfink, *J. Solid State Chem.* **1974**, *9*, 6–14.
[14] J. Iglesias, K. Pachali, H. Steinfink, *Mater. Res. Bull.* **1972**, *7*, 1247–1258.
[15] H. G. von Schnering, R. Hoppe, *Z. Anorg. Allg. Chem.* **1961**, *312*, 99–109.
[16] I. E. Grey, H. Steinfink, *J. Am. Chem. Soc.* **1970**, *92*, 5093–5095.
[17] F. Feher in *Handbook of Preparative Inorganic Chemistry* (Ed: G. Brauer), 2nd ed., Academic Press, New York, **1963**, p. 360.
[18] *PADV Diffraction System Users' Manual 1.0*, Scintag, Santa Clara (CA) **1987**.
[19] A. C. Larson, R. B. Von Dreele, *General Structure Analysis System Software*, University of California, **1994**.
[20] J. Vassiliou, M. Hornbostel, R. Ziebarth, F. J. DiSalvo, *J. Solid State Chem.* **1989**, *81*, 208–216.
[21] J. B. Parise, *Acta Crystallogr. Sect. B* **1980**, *36*, 1179–1180.
[22] a) D. B. McWhan, M. Marezo, J. P. Remeika, P. D. Dernier, *Phys. Rev. B* **1972**, *5*, 2552–2554; b) J. T. Sparks, T. Komoto, *J. Appl. Phys.* **1968**, *39*, 715.
[23] H. H. Kilkmeijer, A. L. T. Moesveld, *Z. Kristallogr.* **1931**, *80*, 91–102.
[24] M. E. Fleet, *Acta Crystallogr. Sect. B* **1972**, *28*, 1237–1241.
[25] G. Collin, C. Chavant, R. Comes, *Acta Crystallogr. Sect. B* **1983**, *39*, 289–296.
[26] The parameters used in the calculations are (in the order H_{ii} [eV], ζ_1, ζ_2, C_1, C_2): Ba 6s: −5.2, 1.5; Ba 6p: −3.2, 1.5; Ni 4s: −7.8, 2.1; Ni 4p: −3.7, 2.1; Ni 3d: −9.9, 5.75, 2.0, 0.5683, 0.6292; S 3s: −20.0, 1.817; S 3p: −13.3, 1.817. 84 k points were used in the irreducible wedge.
[27] a) R. Hoffmann in *Solids and Surfaces: A Chemist's View of Bonding in Extended Structures*, VCH, New York, **1988**; b) T. A. Albright, J. K. Burdett, M.-H. Whangbo in *Orbital Interactions in Chemistry*, John Wiley, New York, **1985**.
[28] A. M. Clark in *Hey's Mineral Index*, The Natural History Museum, London, **1993**, p. 183.
[29] L. H. Fuchs, *Science* 1966, *153*, 166–167.
[30] J. Riley, *Neues Jahrb. Min. Monatsh.* **1978**, *10*, 433.
[31] O. Knop, C. Huang, K. I. G. Reid, J. S. Carlow, F. W. D. Woodhams, *J. Solid State Chem.* **1976**, *16*, 97–116.
[32] J. E. Greedan in *Magnetic Properties of Non-Metals* in *Landolt–Börnstein New Series, Vol. III/27g* (Ed: H. P. J. Wijn), Springer, Heidelberg, **1992**.
[33] B. Martínez, A. Labarta, R. Rodríguez-Solá, X. Obradors, *Phys. Rev. B* **1994**, *50*, 15779–15786.
[34] B. Martínez, F. Sandiumenge, I. Golosovski, S. Galí, A. Labarta, X. Obradors, *Phys. Rev. B* **1993**, *48*, 16440–16448.
[35] R. Ballou, J. Deportes, R. Lemaire, B. Ouladdiaf, *J. Appl. Phys.* **1988**, *63*, 3487–3489.
[36] I. Hase, N. Shirakawa, Y. Nishihara, *J. Phys. Soc. Jpn.* **1995**, *64*, 2533–2540.

  0947-6539/97/0311-1889 $ 17.50+.50/0